EUROPEAN ORGANIZATION FOR NUCLEAR RESEARCH

CERN-PPE/90-105
July 20th, 1990

A MEASUREMENT OF TWO-JET DECAYS OF THE W AND Z BOSONS AT THE CERN $\bar{p}p$ COLLIDER

The UA2 Collaboration

Bern - Cambridge - CERN - Heidelberg - Milano -
Orsay (LAL) - Pavia - Perugia - Pisa - Saclay (CEN)

J.Alitti[10], R.Ansari[6], R.E.Ansorge[2], D.Autiero[9], P.Bareyre[10], G.Blaylock[3], P.Bonamy[10], M.Bonesini[5,3], K.Borer[1], M.Bourliaud[10], D.Buskulic[6], G.Carboni[9], D.Cavalli[5], V.Cavasinni[9], P.Cenci[8], J.C.Chollet[6], C.Conta[7], G.Costa[5], F.Costantini[9,3], A.Cravero[5], A.Dell'Acqua[7], T.DelPrete[9], R.S.DeWolf[2], L.DiLella[3], G.F.Egan[3,a], K.F.Einsweiler[3], L.Fayard[6], A.Federspiel[1], R.Ferrari[7], M.Fraternali[7,b], D.Froidevaux[6], G.Fumagalli[3,7], J.M.Gaillard[6], F.Gianotti[5], O.Gildemeister[3], C.Gössling[3,c], V.G.Goggi[3,7], S.Grünendahl[4], K.Hara[1,d], S.Hellman[3], E.Hugentobler[1], K.Hultqvist[3], E.Iacopini[9,e], J.Incandela[3], K.Jakobs[3], P.Jenni[3], E.E.Kluge[4], N.Kurz[4], S.Lami[4,9], P.Lariccia[8], M.Lefebvre[2,3], L.Linssen[3], M.Livan[7,f], P.Lubrano[3], C.Magneville[10], L.Mandelli[5], L.Mapelli[3], M.Mazzanti[5], K.Meier[3], B.Merkel[6], J.P.Meyer[10], M.Moniez[6], R.Moning[1], M.Morganti[9,g], L.Müller[1], D.J.Munday[2], C.Onions[3], T.Pal[3,1], M.A.Parker[3], G.Parrour[6], F.Pastore[7], E.Pennacchio[7], J.M.Pentney[2], M.Pepe[8], L.Perini[5,b], C.Petridou[9], P.Petroff[6], H.Plothow-Besch[4], G.Polesello[5,3], A.Poppleton[3], K.Pretzl[1], M.Primavera[9,h], M.Punturo[8], L.Rasmussen[3], J.P.Repellin[6], A.Rimoldi[7], P.Scampoli[8], J.Schacher[1], V.Simak[3,i], S.L.Singh[2], S.Stapnes[3], A.V.Stirling[10], F.Tondini[9,8], S.N.Tovey[3,a], E.Tsesmelis[a], G.Unal[6], M.Valdata-Nappi[9,h], V.Vercesi[3,7], A.R.Weidberg[3], P.S.Wells[2], T.O.White[2], D.R.Wood[3], S.A.Wotton[2], H.Zaccone[10]

(submitted to Zeitschrift für Physik C)

Abstract

A study of the two-jet mass spectrum measured with the UA2 calorimeter has revealed a signal from hadronic decays of W and Z bosons above a large background. Production and decay properties of the signal have been measured. The combined production cross-section $\sigma \cdot B(W,Z \rightarrow$ two jets) is 9.6 ± 2.3(stat.) $\pm$ 1.1(syst.) nb, compared with an expectation of 5.9 nb calculated to order α_s^2. A limit on the production cross-section of additional heavy vector bosons decaying into two jets is given as a function of the boson mass.

1 Laboratorium für Hochenergiephysik, Universität Bern, Sidlerstraße 5, 3012 Bern, Switzerland
2 Cavendish Laboratory, University of Cambridge, Cambridge, CB3 0HE, UK
3 CERN, 1211 Geneva 23, Switzerland
4 Institut für Hochenergiephysik der Universität Heidelberg, Schröderstraße 90, 6900 Heidelberg, FRG
5 Dipartimento di Fisica dell'Università di Milano and Sezione INFN Milano, 20133 Milano, Italy
6 Laboratoire de l'Accélérateur Linéaire, Université de Paris-Sud, 91405 Orsay, France
7 Dipartimento di Fisica Nucleare e Teorica, Università di Pavia and INFN, Sezione di Pavia, Via Bassi 6, 27100 Pavia, Italy
8 Dipartimento di Fisica dell'Università di Perugia and INFN, Sezione di Perugia, via Pascoli, 06100 Perugia, Italy
9 Dipartimento di Fisica dell'Università di Pisa and INFN, Sezione di Pisa, Via Livornese, S.Piero a Grado, 56100 Pisa, Italy
10 Centre d'Etudes Nucléaires de Saclay, 91191 Gif-sur-Yvette Cedex, France
a) Visitor from the University of Melbourne, Parkville, Australia 3052
b) Now at Istituto di Fisica, Università di Palermo, Italy
c) Now at Institut für Physik, Universität Dortmund, FRG
d) Now at University of Tsukuba, Tsukuba, Ibaraki 305, Japan
e) Also at Scuola Normale Superiore, Pisa, Italy
f) Now at Dipartimento di Fisica, Università di Cagliari, Italy
g) Now at Dipartimento di Fisica e INFN di Bologna, Università Bologna, Italy
h) Now at Dipartimento di Fisica dell'Università della Calabria e gruppo INFN, Cosenza, Italy
i) Visitor from the Institute of Physics of CSAV, Praha, Czechoslovakia

1. INTRODUCTION

Hadronic jets represent the dominant contribution to high transverse momentum processes in proton-antiproton collisions. High-$p_\perp$ jets were observed in the early phase of experimentation at the CERN $\bar{p}p$ collider [1] and their production properties are successfully described by perturbative QCD [2].

Intermediate vector bosons, W and Z, are expected to decay predominantly into quark-antiquark pairs which evolve into jets very similar to those originating from QCD processes. Studies of W and Z bosons at $\bar{p}p$ colliders have therefore been restricted to their leptonic decay modes [2-5] providing a cleaner experimental signature which separates them from hadronic background. The motivations to measure the hadronic decays of W and Z bosons are manifold :

(i) While the properties of Z decays are being thoroughly studied in e^+e^- collisions [6], W bosons are currently the domain of $\bar{p}p$ colliders which provide the only direct access to their hadronic decay properties.

(ii) W and Z decays to quark-antiquark pairs provide a reference signal to verify experimentally the assignment of jets to parent partons. Ambiguities in this assignment do exist due to higher order QCD effects resulting in the production of more than two high-$p_\perp$ partons. Such contributions have recently been calculated to order α_s^3 [7]. Since partons fragment into the experimentally measured hadrons the definition of a jet is no longer unique and requires instead a prescription for which hadrons to include ("jet algorithms"). The observation of a peak in the two-jet mass spectrum provides a direct test of such prescriptions.

(iii) Once the assignment of jets to their parent partons is verified, two- or multi-jet mass distributions can be used to search for new particles using the measured parameters of the W and Z bosons as a calibration ("jet spectroscopy"). Hadronic decay modes may provide the only direct experimental access to a possible right-handed W boson if its leptonic decays are suppressed or inhibited by the large mass of the right-handed neutrino [8].

The similarity between two-jet final states from the weak production and decay of W and Z and those originating from strong parton-parton interactions excludes an analysis on an event-by-event basis. Instead the peak structure from hadronic W and Z decays has to be observed as a departure from the smooth two-jet mass spectrum from QCD processes. The background is expected to exceed the signal by about two orders of magnitude. The mass resolution for two-jet final states in UA2 is of the same order as the mass difference between the W and the Z (about 10 GeV), so that the two peaks cannot be resolved.

A previous UA2 search [9] for W and Z bosons in the two-jet mass spectrum revealed a signal of 632 ± 190 events with shape and position consistent with expectations. The signal size expected from the Standard Model was 340 ± 80 events. The analysis was based on a data sample corresponding to an integrated luminosity of 0.73 pb^{-1}. The present analysis uses data collected during the 1989 collider run, corresponding to a sample 6 times larger of 4.7 pb^{-1}.

The following Section briefly describes the components of the upgraded UA2 detector relevant to this analysis. Section 3 explains the jet identification methods used at the trigger level and in the data analysis. The two-jet mass spectrum is described in Section 4. In Section 5 the production and decay parameters of the signal are determined. A cross-section is given and compared with the Standard Model prediction. A search for additional heavy vector bosons decaying into jet pairs is reported in Section 6.

2. UA2 APPARATUS

The entire UA2 apparatus was upgraded during the years 1985 to 1987. A global overview of the different components can be found in Ref. [10]. In order to handle the high jet production rates down to two-jet invariant masses well below the W mass region with the UA2 trigger and data acquisition system, only data from the calorimeter were recorded, thus keeping the readout time and event size small.

2.1 Calorimetry

This Section summarizes the main features of the UA2 calorimeter relevant to the analysis presented here. A more complete description can be found in Ref. [11].

Calorimetry is provided over the full azimuthal range, $0° < \phi < 360°$ and the pseudorapidity region $|\eta| < 3$. The calorimeters are subdivided into the central calorimeter (CC) covering pseudorapidities $|\eta| < 1$ and two end-cap calorimeters (EC) covering the region $0.9 < |\eta| < 3$.

The CC is segmented into 240 cells subtending 10° in θ and 15° in ϕ. The electromagnetic part is a multilayer sandwich of lead and scintillator 17 radiation lengths deep, while the hadronic part, subdivided into two compartments, is an iron-scintillator sandwich, resulting in a total thickness of 4.5 absorption lengths including the electromagnetic compartment.

Each EC consists of 12 azimuthal modules,each subdivided into 16 cells. While the cells closest to the beam axis ($2.5 < |\eta| < 3.0$ and $2.2 < |\eta| < 2.5$) cover 30° in azimuth, all cells in

the pseudorapidity interval $1.0 < |\eta| < 2.5$ have a segmentation of $\Delta\phi = 15°$ and $\Delta\eta = 0.2$, with one electromagnetic and one hadronic compartment. The cells closest to the beam axis have only hadronic compartments. The electromagnetic compartment is a multi-layer sandwich of lead and scintillator with a total thickness varying from 17.1 to 24.4 radiation lengths depending on the polar angle. The hadronic calorimeter is a multi-layer sandwich of iron and scintillator corresponding to about 6.5 absorption lengths, including the electromagnetic cells. Cells with only hadronic calorimetry cover the pseudorapidity interval $0.9 < |\eta| < 1.0$ to measure the energy of particles which could otherwise escape detection in the interface between EC and CC modules. To minimize dead spaces in the boundaries between two neighbouring EC modules, the modules have been rotated by 50 mr around their symmetry axis normal to the beam.

The initial absolute calibration of the calorimeters was obtained by exposing every cell to beams of electrons, pions and muons of known momenta. The calibration stability was monitored by measuring the calorimeter response to a radioactive source (Co^{60}). The accuracy of this relative response monitoring has been measured by periodic recalibrations of a part of the calorimeter using test-beams. The uncertainty on the absolute calibration was determined to be $\pm$ 1% for the electromagnetic energy scale and $\pm$ 2% for the hadronic energy scale. Since hadronic jets deposit typically one half of their energy in the electromagnetic compartment, the uncertainty on the absolute energy scale of jet fragments is $\pm$ 1.5%.

To optimize the energy resolution for single charged pions, relative weight factors were defined for all compartments in order to compensate (on the average) for the different calorimeter responses to hadrons and photons. The calorimeter weights applied to the electromagnetic cells were 1.18 in the central calorimeter and 1.2 in the end caps. An additional weight of 1.06 was applied to the second hadronic compartment of the central calorimeter to account for hadronic energy leaking through the back of the calorimeter.

This calibration procedure ensures a correct energy measurement for particles with momenta equal to those of the calibration beam. Since a jet fragment typically carries a small fraction of the parent parton momentum, jet energy measurements are sensitive to deviations from calorimeter linearity at low momenta. Test beam measurements performed with the EC calorimeter showed non-linearities at very low hadron momenta (< 1 GeV). For example, only 70% of the total energy of a charged pion with a momentum of 200 MeV is measured in the calorimeter. The test beam results are well reproduced by simulations of hadronic showers based on Ref. [12] justifying the use of such simulation programs for the central calorimeter where no such low momentum beam measurements are available.

2.2 Time-of-Flight Detector (TOF)

Two arrays of 20 scintillation counters at a distance of ± 120 cm from the centre of the collision region cover the pseudorapidity range $2.3 < |\eta| < 4.1$. The layout is described in Ref. [13]. For the analysis presented here, this detector serves two purposes :

(i) In the absence of track reconstruction, the event vertex is determined by measuring the time-of-flight difference between particles emitted along the p and $\bar{p}$ beams. Averaging over the counter surface, a time resolution of 300 ps has been achieved, providing a determination of the event vertex along the beam with a precision of 25 mm r.m.s..

(ii) At the trigger level, the detector selects inelastic $\bar{p}p$ interactions by demanding a coincidence between particles detected in the two arrays at the time of the nominal beam crossing. This coincidence defines a beam-beam interaction signal. The efficiency of this trigger condition depends on the event topology under study and has been measured for two-jet events [14] and W boson production with subsequent decay into $e\nu$ pairs [4]. For the hadronic production and decay of W bosons an efficiency of 98 ± 1% is estimated from the mean of the two measured numbers.

2.3 Luminosity

The luminosity was measured using eight scintillator telescopes at small angles to the beams, four on each side of the detector. These telescopes consisted of pairs of scintillation counters, 8 m and 10 m from the interaction point. Each pair of counters was read out in a timing coincidence, sensitive only to particles travelling outwards from the interaction region at the time of nominal beam crossing. The accumulated rates of these coincidences were used to compute the integrated luminosity using an algorithm accounting for multiple interactions. More details can be found in Ref. [4].

The data sample used in this analysis was collected during the 1989 run and corresponds to an integrated luminosity of 4.66 ± 0.24 pb^{-1}, where the error is dominated by a 4.7% uncertainty on the knowledge of the total cross-section.

3. JET IDENTIFICATION

The trigger used for this analysis consists of two levels, based on calorimeter information and signals from the TOF detector. A detailed technical description of the trigger system can be found in Ref. [15].

The large QCD two-jet cross-section has imposed a trigger strategy based on two different mass thresholds. A "low mass trigger" was used to collect data for two-jet masses exceeding 66 GeV with the full available integrated luminosity of 4.66 pb^{-1}. The mass region down to 48 GeV was sampled by a special "very low mass trigger" which had to be prescaled by a factor of 8 thus corresponding to an effective integrated luminosity of 0.58 pb^{-1}.

The angular distribution of jets originating from decays of heavy vector bosons is expected to be less peaked in the forward directions than the QCD processes dominated by a $\sin^{-4}(\theta/2)$ form (Rutherford scattering). Jet identification has therefore been restricted to the central calorimeter with a more favourable signal to background ratio (see Section 5.4).

The following subsections describe jet identification for the two trigger levels and the final analysis.

3.1 Jet Identification at the First Trigger Level

A first crude selection of two-jet events is obtained in the 3.84 μs interval between two consecutive bunch crossings of the $\bar{p}p$ collider. Jets are measured in 90° wide azimuthal wedges covering the pseudorapidity range of the central calorimeter. A coincidence between two such wedges at opposite azimuth, each with a transverse energy deposition exceeding 17(13) GeV for the "low mass" ("very low mass") trigger, is required at the first level. The trigger decision is obtained from an analog signal representing the sum of individual photomultiplier signals in the azimuthal wedges. A coincidence with a beam-beam interaction signal is also required to suppress backgrounds from beam-halo interactions. This trigger accepted a total of $5.5 \cdot 10^7$ events.

3.2 Jet Identification at the Second Trigger Level

The second level trigger refines the crude jet identification implemented at the first level. Here transverse cell energies are available in digitized form with individual calibration constants applied. Jet transverse energies are measured in rectangular windows of size $\Delta\theta \times \Delta\phi = 70° \times 75°$, corresponding to 7×5 cells in the θ, ϕ plane of the central calorimeter. The size of this fixed jet aperture is based on measurements of the transverse energy flow in two-jet events. The two leading jets found with this definition have to be at opposite azimuth within 30°. Furthermore, the transverse energies have to exceed 13(10) GeV for the "low mass" ("very low mass") trigger for both jets. The second trigger level accepted a total of 10^7 events, which were recorded on tape for analysis.

3.3 Final Jet Identification and Measurement

The reduction by a factor of five provided by the second trigger level is one of the key elements for this analysis. The data written to tape represent a sample of genuine two-jet events for which no further major reduction is possible. The main task of the finally chosen jet definition is to arrive at the best possible energy resolution.

Before applying the jet algorithm, the effective pseudorapidity coverage of the calorimeter cells is calculated for each event using the vertex position along the beam axis as measured by the TOF detector. The window search algorithm from the second trigger level is then repeated in the extended pseudorapidity region $|\eta| < 2$. The rectangular shape of these windows does not reflect the expected rotational symmetry of the energy flow around the jet axis. Therefore the final jet definition collects the transverse energy in cones with a circular cross-section in the η, ϕ plane to account for the distortion expected from the transformation from the rest frame of the decaying boson to the lab system. The jet direction is given by the vector pointing from the vertex to the transverse energy centroid in the jet cone.

The cone size affects the jet energy resolution in two ways. Particles from the fragmentation process emitted at large angles with respect to the parent parton direction are not detected in narrow cones. Wide cones collect particles not assigned to the jet but instead originating from the interaction of spectator partons (these particles are often referred to as the "underlying event"). The two effects are opposite so that an optimized cone size can be found [16]. Based on the studies presented below, jet energies in this analysis are measured in cones defined by $(\Delta\eta^2 + \Delta\phi^2) < 0.64$.

Two methods have been used to optimize the cone size. The first method uses the PYTHIA 4.8 event generator [17] to study directly the line shape of the W boson in its two-jet decay. For this purpose the parameters of the PYTHIA event generator have been tuned using two-jet events taken with the triggers described in the previous two subsections. The tuning enhances the underlying event contribution compared to the default setting of PYTHIA parameters by enabling multiparton interactions down to approximately 1.65 GeV in transverse momentum. The complete set of tuning parameters is given in Ref. [18]. The enhancement of the underlying event directly affects the jet energy resolution for large cone size. The fragmentation of partons was modelled using the standard JETSET 6.3 [19] prescription. The simulation of the calorimeter response to the fragmentation products was based on beam measurements and shower simulations as described in subsection 2.1. Figure 1 shows the mass response function for cone sizes $(\Delta\eta^2 + \Delta\phi^2)$ of 0.26, 0.64 and 1.13 respectively. An expected increase of the overall response with increasing cone size is observed. The narrow cone exhibits a distinct low mass tail resulting from the loss of fragmentation products. Such a tail is reduced for wider cones. The wide cone develops an

excess of high mass events which can be attributed to the expected contamination of particles not belonging to the jet fragmentation. The medium cone size (0.64) shows the largest peak height corresponding to the most favourable signal-to-background ratio when added to a strong interaction background. The results of a fit with a Gaussian resolution function ignoring the non-Gaussian low and high mass tails are summarized in Table 1. Collecting the jet energy in a cone of $(\Delta\eta^2 + \Delta\phi^2) < 0.64$ optimizes the mass resolution in the W,Z boson region. A small but significant worsening of the resolution is observed for narrower and wider cones.

These results have been obtained assuming the Standard Model mixture of 5 quark flavours. In particular 34% of all W decays ($W \rightarrow c\bar{s}$) are expected to contain a heavy quark which, if decaying semileptonically, could result in a different calorimeter response. This effect has been studied by analysing Monte Carlo generated $W \rightarrow u\bar{d}$ and $W \rightarrow c\bar{s}$ decays separately. Resolutions of 10.5% in the former and 10.8% in the latter case were found, with a statistically significant difference. The overall shape of the response function remains however almost unchanged. In particular the low mass tail can be mostly attributed to geometrical losses of particles outside the cone and to calorimeter non-linearities rather than to neutrinos or muons escaping detection.

A second method to optimize the cone size involves two-jet events collected with the "low mass trigger" in the mass range $70 < m_{jj} < 100$ GeV. The transverse momentum of a two-jet system receives contributions from QCD corrections to the simple $2 \rightarrow 2$ scattering process as well as from instrumental uncertainties in the jet measurement. The mean transverse momenta of two-jet systems reconstructed using the three cone sizes defined in the previous paragraph are given in Table 2. A significant minimum is observed for the medium cone size of $(\Delta\eta^2 + \Delta\phi^2) < 0.64$, which again suggests an optimized jet energy resolution. Also important is the comparison with QCD two-jet events simulated using the PYTHIA event generator described above. The good agreement with the data validates the study described above. It should be pointed out, however, that jets studied by this method are dominated by gluon jets produced either in gluon-gluon or quark-gluon scattering processes. Slight differences in the fragmentation of quark and gluon jets are in fact included in the PYTHIA generator, which predicts a mass resolution of 13.2% for $gg \rightarrow gg$ subprocesses to be compared to the 10.7% for $W \rightarrow q\bar{q}'$ decays. Differences between quark and gluon fragmentation are experimentally not yet well established. Nevertheless it may be dangerous to derive the absolute mass resolution for $W \rightarrow q\bar{q}'$ decays from a sample of average jets.

4. TWO JET MASS SPECTRUM

4.1 Data Analysis Cuts

The final jet algorithm described in subsection 3.3 is applied to all events passing the second trigger level. After ordering the reconstructed jets in decreasing transverse energy ($E_\perp^1, E_\perp^2, \ldots$) the following set of cuts is applied:

i) A cut on the position z of the event vertex as measured by the TOF detector

$$-200 \text{ mm} < z < 200 \text{ mm} ;$$

ii) A cut on the polar angles $\cos\theta_{1,2}$ of jet1 and jet2 to retain only jets contained in the acceptance region of the two trigger levels

$$|\cos\theta_1| < 0.6 \text{ and } |\cos\theta_2| < 0.6$$

(this cut corresponds to a value of $|\eta| < 0.7$) ;

iii) A veto on additional jet activity ($E_\perp^3$) to provide an exclusive two-jet sample

$$E_\perp^3 < 20 \text{ GeV} ;$$

iv) A veto on $Z \rightarrow ee$ decays using the electromagnetic energy fractions of the leading two jets (f^1_{em}, f^2_{em}) measured in the calorimeter

$$f^1_{em} < 80 \% \text{ or } f^2_{em} < 80 \% ;$$

The decays $Z \rightarrow \tau\tau$ with a subsequent hadronic decay of at least one of the τ leptons are suppressed by additional branching ratios. Furthermore their reconstructed two-jet mass is not peaked at the Z mass due to the undetected neutrinos.

v) A rejection of jets potentially not fully contained longitudinally with showers starting deep in the calorimeter

$$f^1_{em} > 20 \% \text{ and } f^2_{em} > 20 \%.$$

The strategy behind these cuts is to provide an exclusive, well measured two-jet sample with a well defined detection efficiency for $W,Z \rightarrow q\bar{q}$ decays. The major reduction results from cuts i) and ii) with a two-jet rejection of 11.5% and 35.8%, respectively. Their

efficiency for $W,Z \rightarrow q\bar{q}$ is well defined and will be discussed in Section 5. Cuts iii) to v) reject only 5.2% of the remaining events and introduce very little uncertainty on the efficiency. Finally, a cut of 40 GeV on the invariant mass of the leading two jets reduces the data sample to approximately $4.5 \cdot 10^6$ events, of which $3.6 \cdot 10^6$ events pass the "low mass trigger" corresponding to an observed cross-section of 770 nb. A total of $1.4 \cdot 10^6$ events pass the "very low mass trigger" corresponding to an effective cross-section of 2400 nb taking into account the prescaling factor of 8.

4.2 The Combined Data Sample

The next analysis step combines the two triggers with their different thresholds to obtain a continuous two-jet mass spectrum extending from mass values well below the expected W,Z signal up to the highest accessible masses. The relative bias of the "low mass trigger" with respect to the "very low mass trigger" has been investigated using the data common to both samples. The result is shown in Figure 2. The two trigger samples can be merged at a mass value of 66 GeV. Below that value, and down to 48 GeV, the mass spectrum is sampled with a reduced luminosity of 0.58 pb^{-1} whereas above 66 GeV the full statistics corresponding to 4.66 pb^{-1} is available. Figure 3 shows the final two-jet mass spectrum. After correcting for the prescaling factor in the mass region between 48 GeV and 66 GeV, a total of $1.7 \cdot 10^6$ events enter into this plot corresponding to an observed cross-section of 370 nb for two-jet masses exceeding 48 GeV. There is no obvious structure over the entire mass range covered by this spectrum.

4.3 Evidence for a Signal from W,Z Decays

The expected signal from the decays $W \rightarrow q\bar{q}'$ and $Z \rightarrow q\bar{q}$ corresponds to a cross-section of the order of 1 nb when including all detection efficiencies (see Section 5). To search for this signal in the observed two-jet mass spectrum, which corresponds to an observed cross-section of 370 nb, a statistical analysis has to be applied. The mass spectrum was initially fitted with several monotonically decreasing functions without allowing for structures corresponding to the expected mass resolution. All fits have been performed over the two-jet mass range $48 < m_{jj} < 300$ GeV. It was found that at least 3 parameters are needed for a satisfactory description of the global shape of the QCD continuum. The following two parametrizations have been tried :

i) $m^{-\alpha} \cdot e^{-\beta \cdot m} \cdot e^{-\gamma \cdot m^2}$

ii) $m^{-\alpha} \cdot \ell n(\beta/m) \cdot \ell n(\gamma/m^2)$

Both parametrizations result in approximately the same fit quality. The better result was achieved with parametrization i) corresponding to a χ^2 of 163 for 124 degrees of freedom

(d.o.f.) when fitting the two-jet mass range $48 < m_{jj} < 300$ GeV. The probability for this fit is ~ 1%. Figure 4a shows the experimental data together with the background fit of type i) around the expected W,Z signal. In this form of representation the number of events has been weighted with a mass dependent factor of $(m/100)^6$ to attenuate the steep fall-off of the mass spectrum and to give a realistic size to the statistical error bars. Apparently the low fit probability originates from the mass range $70 < m_{jj} < 100$ GeV where most measured data points are several standard deviations away from the fitted curve. Removing this mass region from the fit does in fact improve the fit quality to $\chi^2 = 97.5$ for 109 d.o.f. corresponding to a probability of 77.6%. Figure 4b presents this fit together with the data. The observed excess of events in the excluded mass range provides clear evidence for hadronic W,Z decays.

5. PRODUCTION AND DECAY CHARACTERISTICS OF THE SIGNAL

5.1 Signal Properties

The analysis procedure has so far not made any assumption about the line shape of the expected signal. A quantitative study of the excess of events observed in the two-jet mass spectrum requires some assumptions.

The mass resolution σ_m of the calorimeter for the decay $W \rightarrow$ two jets is 10.7%, which exceeds by far the natural line width. The experimentally observed line shape has therefore been approximated by a Gaussian resolution function. The effect of non-Gaussian tails in the mass resolution function has to be corrected for in the cross-section measurement.

The masses of the W and Z bosons have recently been measured precisely [5,6]. However, Figure 1 indicates that peaks in the two-jet mass spectrum are expected to shift due to instrumental effects like calorimeter non-linearities, particle losses outside the jet cone, etc. While the absolute mass scale is specific to the experimental approach, these effects are not expected to change the mass ratio between W and Z. All fits assume a mass ratio $m_Z/m_W = 1.13$ based on a recent measurement of the decays $W \rightarrow e\nu$ and $Z \rightarrow ee$ performed with the same calorimeter [5].

The relative contribution from W and Z decays to the observed peak structure is given by the Standard Model after correcting for the relative detection efficiencies. Taking the experimentally observed cross-section ratio of W,Z production in the $Z \rightarrow ee$ and $W \rightarrow e\nu$ decay modes [4], the Standard Model ratios of the W and Z partial widths into quarks and leptons (assuming 5 quark flavours) and the relative detection efficiencies for the $W \rightarrow q\bar{q}'$ and $Z \rightarrow q\bar{q}$ decays, a ratio of 0.397 is expected between the cross-sections for Z and W boson production.

Using these assumptions the observed mass spectrum has been fitted to a function G with 6 free parameters:

$$G = B(\alpha, ß, \gamma) + S(m_W, \sigma_m, N)$$

The role of B is to describe the two-jet continuum from QCD processes. Parametrization (i) (see Section 4.3) has been chosen because it gives the best description of the data outside the signal region. The signal function S is the sum of two Gaussian line shapes with the W boson mass m_W, the mass resolution σ_m and the signal size N as free parameters. The integral of the fit function is normalized to the total amount of observed events in the two-jet mass spectrum. The results of the fit are summarized (case 1) in Table 3 and a representation of the fit together with the data is displayed in Figure 4c. Figure 5a shows the excess of events over the fitted QCD background together with the overall W,Z fit and the contributions from W and Z separately.

The best fit gives a signal of 5618 ± 1334 events, corresponding to a signal to background ratio of 1/38 when integrating the two-jet mass spectrum from 70 GeV to 100 GeV. The statistical significance amounts to 4.2 standard deviations (s.d.). The apparent W mass is 79.2 ± 1.7 GeV. A simulation of W → two jets decays (see Figure 1) and the recent precision measurement of the W mass [5] give an expectation of 74.8 ± 3.4 GeV. The major uncertainties in this prediction arise from the simulation of the underlying event (2 GeV), the calorimeter response to low energy particles (2.5 GeV) and the absolute energy scale of the calorimeter (1.1 GeV). The measured mass resolution of 9.9 ± 2.5 % agrees well with the expectation of 10.7 ± 1.8%. The error on the latter number is due to the underlying event model (1.5%) and the calorimeter response to low energy particles (1.0%). Fixing the mass resolution to its expected value of 10.7% (case 3 in Table 3) increases the statistical significance of the signal to 8.1 s.d. and the reconstructed event number by 12% from 5618 to 6337. The dependence of the measured cross-section on the knowledge of the experimental mass resolution will be discussed in Section 5.3.

The correct evaluation of the statistical significance has been verified by a Monte Carlo method. A simulated W,Z mass peak of 5000 events has been added to a simulated QCD continuum scattering the data points according to their statistical error. The same fit procedure as for the data has been applied to the simulated spectra. Such a Monte Carlo experiment was then repeated 500 times. For the case of 6 free parameters an average significance of 3.6 s.d. with a spread of 1.4 s.d. (r.m.s.) is predicted to be compared to the 4.2 s.d. measured in the real experiment. If the mass resolution is fixed to its generated value a mean significance of 6.7 s.d. with a r.m.s. of 1.5 s.d. is expected, to be compared to the 8.1 s.d. actually observed. Applying a fit with a fixed mass resolution to a simulated QCD continuum only (no W,Z signal) results in an average signal of 34 events reconstructed with a r.m.s. spread

of 997. This shows that a statistical fluctuation of the QCD continuum as large as the observed signal is very improbable.

All fits have been performed using the data sample obtained by combining data from the full statistics trigger for mass values exceeding 66 GeV and from the prescaled trigger for masses below that value. In order to investigate whether the procedure to combine the two data sets introduces any systematic effect we have fitted the prescaled trigger alone. Fitting this data sample and keeping the values for the apparent W mass and the mass resolution at the values determined in the fit to the full data sample, leads to the results presented in Table 3 (case 2). Although limited by statistics the reconstructed signal size is quite compatible with the one obtained from the complete data set.

The relative contributions from W and Z decays have been measured by fixing the expected signal position and the mass resolution in the fit to their observed values. A signal of 5637 ± 958 events is found with a cross-section ratio between the observed Z and W decays of 0.39 ± 0.16. This measurement depends strongly on the assumed peak positions and the mass resolution.

These studies show that a simple double Gaussian model for the line shape position and width of the observed signal is in agreement with the expectations from hadronic W,Z decays.

5.2 Effects of Strong-Electroweak Interference on the Line Shape

Due to QCD-electroweak interference effects in the quark scattering processes, the signal in the two-jet mass distribution is not simply a superposition of W and Z resonances on the rapidly falling QCD continuum as implicitely assumed in the preceding analysis. A detailed study of all interference effects and their manifestation in the experimentally observed two-jet mass distribution has been carried out in Ref. [20]. For a comparison with experimental data this calculation has been convoluted with a Gaussian mass resolution of $\sigma_m = 10\%$. The QCD part (quark-quark scattering mediated by gluon-exchange) has been subtracted leaving a line shape which, in addition to the purely electroweak terms, also contains the QCD-electroweak interference contributions. This line shape has been fitted to the experimental data leaving the W mass, signal size and QCD background as free parameters in the fit. The results are listed in Table 3 (case 4). Figure 5b shows the data after subtracting the QCD background as determined by this fit. The complete fit exhibits two components. Apart from the W,Z resonance, a non-resonant contribution originating from s-channel photon and t-channel vector boson exchange is visible. The total signal size integrated over the full fit range is 8516 ± 1062 events. Of those 2425 can be accounted for by the non-resonant

contribution leaving a resonant signal from W,Z decays of 6091 ± 1062 events. The apparent W mass is measured to be 79.9 ± 1.1 GeV.

The data have also been fitted with the pure s-channel vector boson exchange part of calculation [20]. This approach is in principle equivalent to the one used above where line shape distortions from interference effects and non-resonant contributions are absorbed in the QCD continuum parametrization. The results are listed in Table 3 (case 5) and Figure 5c. A signal of 6805 ± 768 events at a mass value of 78.1 ± 0.7 GeV is observed.

In all of these studies the signal size and the peak position have been left as free parameters in the fit and their relative dependence on line shape parametrizations has been compared with the predictions of Ref. [20]. Explicit subtraction of interference effects and non-resonant contribution instead of absorbing these effects into the QCD background leads to a predicted loss of 8% in signal size and a +2.2 GeV mass shift in the peak position. Experimentally, a signal loss of 11 ± 21% and a mass shift of +1.8 ± 1.3 GeV are observed. Therefore the current measurement is not sensitive to such details of the line shape.

5.3 Cross Section and Comparison with the Standard Model

The number of events found by the fits have been converted to cross-sections by correcting for various efficiency factors. The combined efficiency of the two trigger levels has been evaluated using the PYTHIA event generator to simulate both W → two jets and Z → two jets decays. The efficiencies found for W and Z are 35.0% and 39.3% respectively. The difference of 4.3% arises mostly from the mass difference leading to more central production of Z bosons compared to W's. A combined W,Z efficiency of 36.7% is deduced using the expected cross-section ratio between W's and Z's. This number has been assigned a systematic error of 2.9% receiving contributions from the underlying event model, uncertainties in the low energy response of the calorimeter and the fragmentation model.

The efficiency of the TOF detector for $\bar{p}p$ interactions containing hadronic production and decay of W,Z bosons is 98 ± 1% as described in subsection 2.2.

The efficiency of the analysis cuts has been evaluated using PYTHIA. It amounts to 45.0% for both W's and Z's. The uncertainty on this number is 1.4% originating mostly from the veto against a third jet and from the condition of good longitudinal jet containment in the calorimeter.

In addition, the vertex cut keeps only 88.5% of the two-jet events used in this analysis.

The possibility of a bias introduced by the fitting procedure has been studied using the Monte Carlo technique described in subsection 5.1. The fraction of events reconstructed in the mass peak compared to those generated was found to be 96.9 ± 3.5% when fitting the data with the mass resolution as a free parameter and 99.1 ± 0.7% when fixing it to its generated value. The errors are determined by the number of Monte Carlo experiments performed. It should be noted that this number is a measurement of a possible systematic under- or overestimate of the signal size which could in principle exceed 100%.

A final source of inefficiency is caused by the fact that the response curve of Figure 1b is fitted using a Gaussian resolution function which is unable to account for the observed low mass tail. This effect has been estimated by fitting the predicted response function with a Gaussian line shape and by measuring the fraction seen in the fit. The efficiency factor assigned to this effect is 90.7 ± 3.8 %.

A summary of all efficiencies can be found in Table 4. When leaving the mass resolution as a free parameter the overall detection efficiency for W,Z → two jets is 12.6 ± 1.3%. For a fixed resolution the corresponding value is 12.9 ± 1.2%.

For the case of a 6 parameter fit to a double Gaussian resolution function the corrected cross-section is $\sigma \cdot B(W,Z \rightarrow \text{two jets}) = 9.6 \pm 2.3(\text{stat.})$ nb. Fixing the mass resolution to its expected value results in a smaller statistical error: $\sigma \cdot B(W,Z \rightarrow \text{two jets}) = 10.5 \pm 1.3(\text{stat.})$ nb.

Three sources of systematic errors have to be considered. The error on the integrated luminosity amounts to 5.2%. The relative uncertainty on the overall efficiency is 10.2% for the case of an unconstrained mass resolution and 9.6% for a fixed mass resolution. Fixing the mass resolution to its expected value introduces an additional uncertainty, which has been evaluated by varying the resolution in the range from 8.9% to 12.5% corresponding to its estimated uncertainty and repeating the fit. The observed signal size varies by as much as 21.5%. The final results for the cross-sections are :

$$\sigma \cdot B(W,Z \rightarrow \text{two jets}) = 9.6 \pm 2.3(\text{stat.}) \pm 1.1(\text{syst.}) \text{ nb}$$
for a free mass resolution ;

$$\sigma \cdot B(W,Z \rightarrow \text{two jets}) = 10.5 \pm 1.3(\text{stat.}) \pm 2.5(\text{syst.}) \text{ nb}$$
for a fixed mass resolution.

These results show that the enhanced statistical significance of the second method is weakened by the lack of precise knowledge of the two-jet mass resolution. Thus the two methods give results of comparable overall precision.

The measurements have been compared to Standard Model predictions. The production cross-section has been calculated at the Born level, to order α_S [21] and partially to order α_S^2 [22]. In the calculations the Z mass was taken to be 91.15 GeV [6]. The recent UA2 measurement of m_W/m_Z [5] was used to compute the weak mixing angle $\sin^2\theta_W$ and to derive the W mass. The structure functions were taken from DFLM with Λ_{QCD} = 160 MeV [23]. The uncertainty arising from the choice of structure functions amounts typically to ±10% and is not considered further in the comparison. To derive a value for the strong coupling constant α_S, the QCD scale parameter Λ_{QCD} used in the structure functions has been reduced from 160 MeV to 101.5 MeV. This procedure assures a smooth evolution of α_S from the low Q^2 region used for the evaluation of structure functions (4 quark flavours) to the high Q^2 values of $Q^2 = m_W^2$ (m_Z^2) relevant for the processes under study (5 quark flavours). For the evaluation of the branching fractions $B(Z \to q\bar{q})$ and $B(W \to q\bar{q}')$ the decays $Z \to t\bar{t}$ and $W \to t\bar{b}$ were not allowed in view of recent limits on the top quark mass [24]. The partial hadronic widths of the W and Z bosons have been corrected for QCD effects to order α_S. The branching fractions used are $B(W \to q\bar{q}') = 67.6\%$ and $B(Z \to q\bar{q}) = 70.3\%$.

Predictions for $\sigma \cdot B(W,Z \to q\bar{q})$ at 3 different perturbation orders of the cross-section calculations are summarized in Table 5. The measured cross-sections are about 1.5 s.d. larger than the $O(\alpha_S^2)$ calculation of 5.8 nb.

The UA2 Collaboration has recently measured the production cross sections of W and Z bosons in their electron decay modes [4] :

$$\sigma \cdot B(W \to e\nu) = 0.660 \pm 0.015 \text{ (stat.)} \pm 0.037 \text{ (syst.) nb}$$
$$\sigma \cdot B(Z \to ee) = 0.0704 \pm 0.0055 \text{ (stat.)} \pm 0.0040 \text{ (syst.) nb}$$

A direct comparison with these measurements avoids theoretical uncertainties arising from structure functions and QCD corrections to the production processes. The experimental uncertainties of the cross-section measurements in jet and electron decay modes are however of different nature and have to be taken into account in the comparison. A partial cancellation of uncertainties in the integrated luminosities has little effect on the experimental error. The following ratio, expected to be unity in the Standard Model, has been calculated :

$$R = \frac{\sigma \cdot B(W,Z \to q\bar{q})}{\sigma \cdot B(W \to e\nu) \cdot \frac{\Gamma(W \to q\bar{q}')}{\Gamma(W \to e\nu)} + \sigma \cdot B(Z \to ee) \cdot \frac{\Gamma(Z \to q\bar{q})}{\Gamma(Z \to ee)}}$$

The ratios of the partial decay widths into quarks and leptons have been taken from the Standard Model using the parameters given above. Their values are

$$\frac{\Gamma(W \rightarrow q\bar{q}')}{\Gamma(W \rightarrow e\nu)} = 6.25$$

$$\frac{\Gamma(Z \rightarrow q\bar{q})}{\Gamma(Z \rightarrow ee)} = 21.1$$

The experimental value obtained for the ratio R is 1.71 ± 0.45. Again, the agreement with the expectation of unity is within 1.6 s.d. The experimental error combines statistical and systematic uncertainties and is dominated by the contribution from the $\sigma \cdot B(W,Z \rightarrow$ two jets) measurement.

5.4 Decay Angular Distribution

Apart from a measurement of the total cross-section, a study of differential distributions is of interest to validate further the observed signal. The accuracy of such measurements will obviously be limited by the size of the observed signal. Nevertheless, an attempt has been made to measure the angular distribution of the decay jets in the W,Z centre of mass system. This distribution is (at least in principle) expected to differentiate between vector boson decays and Rutherford-type angular distributions as expected for gluon-gluon scattering.

The angular distribution of the observed signal has been measured in three $|\cos\theta^*|$ bins. Peak position and mass resolution for the fit procedure have been fixed to the values obtained from the integrated sample in order to improve the significance of the differential measurements (these numbers are not expected to depend on the decay angle). The individual measurements performed in the three $|\cos\theta^*|$ bins have been corrected for trigger and cut efficiency assuming an angular distribution expected for $W \rightarrow q\bar{q}'$ decays. All other efficiency factors are expected to be independent of angle and are ignored in the angular distribution which has been normalized to unity in the region $|\cos\theta^*| < 0.6$. Figure 6 shows the measured data points together with the expectations for $gg \rightarrow gg$ processes and $W \rightarrow q\bar{q}'$ decays. The curves have been plotted with the same normalization as the experimental data in the region $|\cos\theta^*| < 0.6$.

Although the experimental data cannot distinguish between the two distributions, the $\cos\theta^*$ dependence of the observed signal is consistent with expectation. Moreover, Figure 6 justifies the use of central rapidities for this analysis, because the expected signal to background ratio rapidly decreases in the forward direction.

6. SEARCH FOR ADDITONAL HEAVY VECTOR BOSONS DECAYING INTO TWO JETS

A search for additional heavy vector bosons X decaying to two-jet final states has been carried out in the range from the W,Z mass region up to 300 GeV. The mass spectrum has been fitted to a single Gaussian resolution function added to a QCD background parametrized as for the W,Z $\rightarrow$ two jets analysis. For a given mass the fit has been performed using the expected mass resolution obtained from the PYTHIA event generator. The mass resolution improves from 10.7% in the W,Z mass region to 8.4% for masses around 300 GeV. At even higher masses the resolution degrades again due to longitudinal losses of hadronic showers.

The fit results have been corrected for the detection efficiency to obtain a 90% C.L. limit on $\sigma \cdot B(X \rightarrow \text{two jets})$ as a function of the two-jet mass. The combined trigger and experimental cut efficiency rises from 16.5% in the W,Z mass region to 19.9% for masses around 300 GeV. All other efficiencies are independent of the produced mass and are taken from the W,Z $\rightarrow$ two jets analysis (Table 4).

Systematic errors on the integrated luminosity, the efficiency factors and the mass resolution have been taken from the W,Z cross-section measurement described in the previous Section. The cross-section limit on the production of a new particle at a given mass receives an additional systematic uncertainty from possible shifts of the two-jet mass scale. The actual observation of the W,Z peaks in the same mass spectrum provides a calibration signal. The apparent position of this peak and its error have been used to estimate an uncertainty of 11% on the cross-section from this source. The dominant source of systematic uncertainty in this measurement is therefore again given by the limited knowledge of the two-jet mass resolution, which amounts to as much as 21.5%.

The W,Z mass region requires a special treatment due to the presence of the signal from the known vector bosons. To be conservative, a signal described by the measured line shape parameters and of a size expected from the $O(\alpha_s)$ calculation (Table 5) has been subtracted from the observed two-jet mass spectrum before applying the fit.

The result is given in Figure 7. The dashed line indicates the expected signal from an additional W boson calculated using the partial $O(\alpha_s^2)$ calculation [22] with Standard Model couplings. The set of DFLM structure functions corresponding to $\Lambda_{QCD} = 360$ MeV [23] was used because it predicts the lowest cross-section of all DFLM structure function sets. Analog to the procedure explained in subsection 5.3 the effective Λ_{QCD} has been reduced to assure a smooth evolution of α_s when passing the threshold from 4 quark flavours to 5 quark flavours. A mass independent branching fraction of 67.6% corresponding to 5 quark

flavours was used. This prescription serves only as one specific example for a process which is in principle accessible through this channel. In particular the branching fraction depends on the particle content of the model under study. The model shown here can only be excluded in the mass region 101 GeV $< m_{jj} <$ 158 GeV. At the low mass end the excess of events over the $O(\alpha_s)$ expectation does not allow to exclude an additional vector boson. At the high mass end the measurement is limited by statistics.

In conclusion the method of jet spectroscopy has only given rather weak constraints on the production of additional vector bosons. The proximity of the upper bound to the expected cross-section does however motivate future efforts in this direction. Multi-jet spectroscopy can serve as a powerful tool in the search for new particles only directly accessible through this decay mode [8]. The limiting factors of this experiment are the two-jet mass resolution, the lack of precise knowledge of this resolution and the available statistics. Experiments at future colliders may improve in all these respects [16].

7. CONCLUSIONS

This paper has successfully demonstrated the feasibility of two-jet mass spectroscopy at hadron colliders. The observed signal of hadronic W,Z decays has been studied with respect to its line shape, size and decay characteristics. Agreement with the Standard Model has been found. The combined production cross-section $\sigma \cdot B(W,Z \rightarrow q\bar{q})$ is 9.6 $\pm$ 2.3(stat.) $\pm$ 1.1(syst.) nb to be compared with an expectation of 5.8 nb calculated to $O(\alpha_s^2)$. This analysis has also established limits on the production of additional heavy vector bosons decaying to two-jet final states.

ACKNOWLEDGEMENTS

We gratefully acknowledge P. Darriulat for his contributions and guidance during the design and construction of the UA2 upgrade project.

The technical staff of the institutes collaborating in UA2 have contributed substantially to the construction and operation of the experiment. We deeply thank them for their continuous support. The experiment would not have been possible without the very successful operation of the improved CERN $\bar{p}p$ Collider whose staff and coordinators we sincerely thank for their collective effort.

We thank U.Baur, E.W.N. Glover and A.D. Martin for helpful discussions and for making their calculations on QCD-electroweak interference effects available to us. We also thank B. Webber for fruitful discussions.

Financial support from the Schweizerischen Nationalfonds zur Förderung der Wissenschaftlichen Forschung to the Bern group, from the UK Science and Engineering Research Council to the Cambridge group, from the Bundesministerium für Forschung und Technologie to the Heidelberg group, from the Institut National de Physique Nucléaire et de Physique des Particules to the Orsay group, from the Istituto Nazionale di Fisica Nucleare to the Milano, Pavia, Perugia and Pisa groups and from the Institut de Recherche Fondamentale (CEA) to the Saclay group are acknowledged.

TABLE 1

Two-jet mass resolutions predicted by the PYTHIA Monte Carlo for three different cone sizes.

cone size ($\Delta\eta^2 + \Delta\phi^2$)	σ_m ($W \rightarrow q\bar{q}'$, MC) (%)
0.28	11.3
0.64	10.7
1.13	11.4

TABLE 2

Transverse momenta of two-jet events (data and PYTHIA Monte Carlo) in the mass region 70 GeV < m_{jj} < 100 GeV for three different cone sizes.

cone size ($\Delta\eta^2 + \Delta\phi^2$)	$\langle p_\perp \rangle$ data (GeV)	$\langle p_\perp \rangle$ MC (GeV)
0.28	10.26	10.26
0.64	9.75	9.92
1.13	10.25	10.15

TABLE 3

Summary of fit results. The five different cases are explained in the text.

case	1	2	3	4	5
background parameters					
α	7.78±0.02	7.89±0.05	7.88±0.02	8.10±0.02	7.99±0.02
$\beta(\times 10^2)$	-2.93±0.04	-3.28±0.12	-3.14±0.04	-3.65±0.04	-3.42±0.04
$\gamma(\times 10^5)$	8.17±0.18	9.62±0.48	8.64±0.16	9.93±0.16	9.34±0.17
signal parameters					
N (events)	5618±1334	5165±1810	6337±783	6091±1062	6805±768
σ_m (%)	9.9±2.5	9.9 (fixed)	10.7 (fixed)	10.0 (fixed)	10.0 (fixed)
m_W (GeV)	79.2±1.7	79.2 (fixed)	78.1±1.0	79.9±1.1	78.1±0.7
χ^2/N.D.F.	114 / 121	83 / 123	113 / 122	115 / 122	113 / 122

TABLE 4

Contributions to the detection efficiency for W,Z → two jets

source	efficiency (%)
jet trigger	36.7±2.9
TOF condition	98.0±1.0
analysis cuts	45.0±1.4
vertex cut	88.5
fit method (resolution free)	96.9±3.5
fit method (resolution fixed)	99.1±0.7
Gaussian line shape	90.7±3.8
overall (res. free)	12.6±1.3
overall (res. fixed)	12.9±1.2

TABLE 5

Comparison of the measured cross-sections with calculations performed up to three different perturbative orders.

	$\sigma \cdot B(W,Z \rightarrow q\bar{q})$ (nb)
data (free mass resolution)	9.6±2.3(stat.)±1.1(syst.)
data (fixed mass resolution)	10.5±1.3(stat.)±2.5(syst.)
Born level	4.2
α_s correction included	5.3
α_s^2 correction partially included	5.8

REFERENCES

[1] UA2 Collaboration, M. Banner et al., Phys. Lett. B118 (1982) 203;
UA1 Collaboration, G. Arnison et al., Phys. Lett. B123 (1983) 115.

[2] For a review see: P. Bagnaia and S.D. Ellis, Ann. Rev. Nucl. Part. Sc. 38 (1988) 659 (also for previous references).

[3] CDF Collaboration, F. Abe et al., Phys. Rev. Lett. 63 (1989) 720;
CDF Collaboration, F. Abe et al., Phys. Rev. Lett. 64 (1990) 152.

[4] UA2 Collaboration, J. Alitti et al., Measurement of W and Z Production Cross Sections at the CERN $\bar{p}p$ Collider, CERN-EP/90-20, to be published in Z. Phys. C.

[5] UA2 Collaboration, J. Alitti et al., Phys. Lett. B241 (1990) 150.

[6] MARK II Collaboration, G. Abrams et al., Phys. Rev. Lett. 63 (1989) 2173;
ALEPH Collaboration, D. Decamp et al., Phys. Lett. B231 (1989) 519 and B235 (1990) 399;
DELPHI Collaboration, P. Aarnio et al., Phys. Lett. B231 (1989) 539 and B241 (1990) 435;
L3 Collaboration, B. Adeva et al., Phys. Lett. B231 (1989) 509 and B237 (1990) 136;
OPAL Collaboration, M.Z. Akrawy et al., Phys. Lett. B231 (1989) 530 and B240 (1990) 497.

[7] S.D. Ellis, Z. Kunszt, D.E. Soper, Phys. Rev. Lett. 64 (1990) 2121;
F. Aversa, P. Chiappetta, M. Greco, J.P. Guillet, LNF-90/012 PT, March 1990.

[8] P. Langacker and Uma S. Sankar, Phys. Rev. D40 (1989) 1569.

[9] UA2 Collaboration, R. Ansari et al., Phys. Lett. 186B (1987) 452.

[10] UA2 Collaboration, CERN/SPSC 84-30, 84-95 (1984) and 85-3 (1985), unpublished;
UA2 Collaboration, C.N. Booth, Proc. 6th Topical Workshop on Proton-Antiproton Collider Physics, Aachen, 1986, eds. K. Eggert et al., (World Scientific, Singapore, 1987) 381.

[11] A. Beer et al., Nucl. Inst. Meth. 224 (1984) 360;
F. Alberio, et al.,The Electron, Jet and Missing Transverse Energy Calorimetry of the upgraded UA2 experiment at the CERN $\bar{p}p$ Collider, in preparation for Nucl. Inst. Meth..

[12] H.C. Fesefeldt, Simulation of Hadronic Showers, PITHA 85-02, Aachen 1985.

[13] T. Koch, Aufbau und Test eines Flugzeitsystems, HD-IHEP 89-05, Heidelberg 1989.

[14] UA2 Collaboration, J. Alitti et al., Phys. Lett. B235 (1990) 363.

[15] P. Baehler et al., Proc. of the International Conference on the Impact of Digital Microelectronics and Microprocessors on particle Physics 1988, eds. M. Budinich et al. (World Scientific, Singapore, 1988) 245;
G. Blaylock et al., Proc. of the International Conference on the Impact of Digital Microelectronics and Microprocessors on particle Physics 1988, eds. M. Budinich et al. (World Scientific, Singapore, 1988) 247.

[16] The LHC jet study group, T. Åkesson et al., ECFA 84/89, CERN 84-10, September 1984.

[17] H. Bengtsson and T. Sjostrand, The Lund Monte Carlo for Hadronic Processes, LUTP 87-3, UCLA-87-001.

[18] The PYTHIA event generator has been modified to allow for multiple interactions assuming a varying impact parameter and a hadronic matter overlap consistent with a double Gaussian matter distribution. The cross-section for this process has a continuus turnoff at 1.65 GeV. The list of PYTHIA parameters changed from their default values is : IPY(3) = 12, IPY(12) = 4, IPY(17) = 3, PYPAR(32) = 1.65.

[19] T. Sjostrand and M. Bengtsson, The Lund Monte Carlo for Jet Fragmentation and e^+e^- Physics, LUTP 86-22 (1986).

[20] U. Baur, E.W. Glover, A.D. Martin, Phys. Lett. B232 (1989) 519 and references therein;
B. Webber, private communication.

[21] G. Altarelli et al., Z. Phys. C27 (1985) 617.

[22] T. Matsuura, Higher Order Corrections to the Drell-Yan process, Ph. D. Thesis, University of Leiden, 1989;
T. Matsuura and W.L. van Neerven, Z. Phys. C38 (1988) 623;
T. Matsuura, S.C. van der Marck and W.L. van Neerven, Phys. Lett. B211 (1988) 171 and Nucl. Phys. B319 (1989) 570.

[23] M. Diemoz et al., Z. Phys. C39 (1988) 21.

[24] CDF Collaboration, F. Abe et al., Phys. Rev. Lett. 64 (1990) 142;
CDF Collaboration, F. Abe et al., Phys. Rev. Lett. 64 (1990) 147;
UA2 Collaboration, T. Åkesson et al., Z. Phys. C46 (1990) 179.

FIGURE CAPTIONS

Fig. 1 Mass response function for $W \rightarrow q\bar{q}'$ decays generated with PYTHIA. The 3 plots contain the same number of events.
The dotted line indicates the peak height reached with the optimized cone size of $(\Delta\eta^2 + \Delta\phi^2) < 0.64$.
a) Cone size for jet reconstruction $(\Delta\eta^2 + \Delta\phi^2) < 0.28$
b) Cone size for jet reconstruction $(\Delta\eta^2 + \Delta\phi^2) < 0.64$
c) Cone size for jet reconstruction $(\Delta\eta^2 + \Delta\phi^2) < 1.13$

Fig. 2 Bias of the "low mass trigger" with respect to the "very low mass trigger" as a function of the two-jet mass. The right arrow indicates the lowest non biased mass value. The left arrow indicates the mass cut-off in the analysis below which no data are available.

Fig. 3 The final two-jet mass spectrum. The first nine data points on the low mass side are from the "very low mass trigger" and have been scaled up by the prescaling factor of 8.

Fig. 4 The two-jet mass spectrum in the region around the expected W,Z signal ($48 < m_{jj} < 138$ GeV). The vertical axis presents the number of observed events in a 2 GeV wide mass bin weighted by factors $(m/100)^6$. Three different fits have been overlayed on the data:
a) Background fit performed over the full mass range
b) Background fit excluding the mass range $70 < m_{jj} < 100$ GeV
c) Combined fit to QCD background and the W,Z signal described by 3 free parameters as explained in the text. The dashed line represents the background contribution only.

Fig. 5 The two-jet mass spectrum in the region around the W,Z signal after subtraction of the fitted QCD background.
a) Fit performed with a double Gaussian resolution function leaving the resolution as a free parameter. The full line represents the combined W,Z signal. The dashed lines show the contributions from W and Z separately.
b) Fit performed taking into account the complete set of $q\bar{q}' \rightarrow q\bar{q}'$ amplitudes according to Ref. [20] subtracting out the contribution from strong interaction. The full line represents the complete fit. The dashed line shows the non-resonant contribution originating from s-channel photon and t-channel vector boson exchange. The dashed- dotted line stands for the s-channel vector boson exchange only.

c) The full line represents the fit performed using only the s-channel vector boson exchange part of calculation [20]

Fig. 6 The angular distribution of the observed W,Z signal in the two-jet center-of-mass system. The full line represents the distribution expected for $W \rightarrow q\bar{q}'$ decays. The dashed line is the expectation for the QCD subprocess $gg \rightarrow gg$ (Rutherford scattering). The distributions are normalized in the region $0 < |\cos\theta^*| < 0.6$ in which the experimental data are observed.

Fig. 7 Upper bound on the production cross-section for a heavy vector particle X in the two-jet decay mode (90% C.L.). In the W,Z mass region a signal described by the measured line shape parameters and of a size expected from the $O(\alpha_s)$ calculation has been subtracted from the observed mass spectrum. The dashed curve represents the expectation from a W' boson assuming 5 quarks in the two-jet decay.

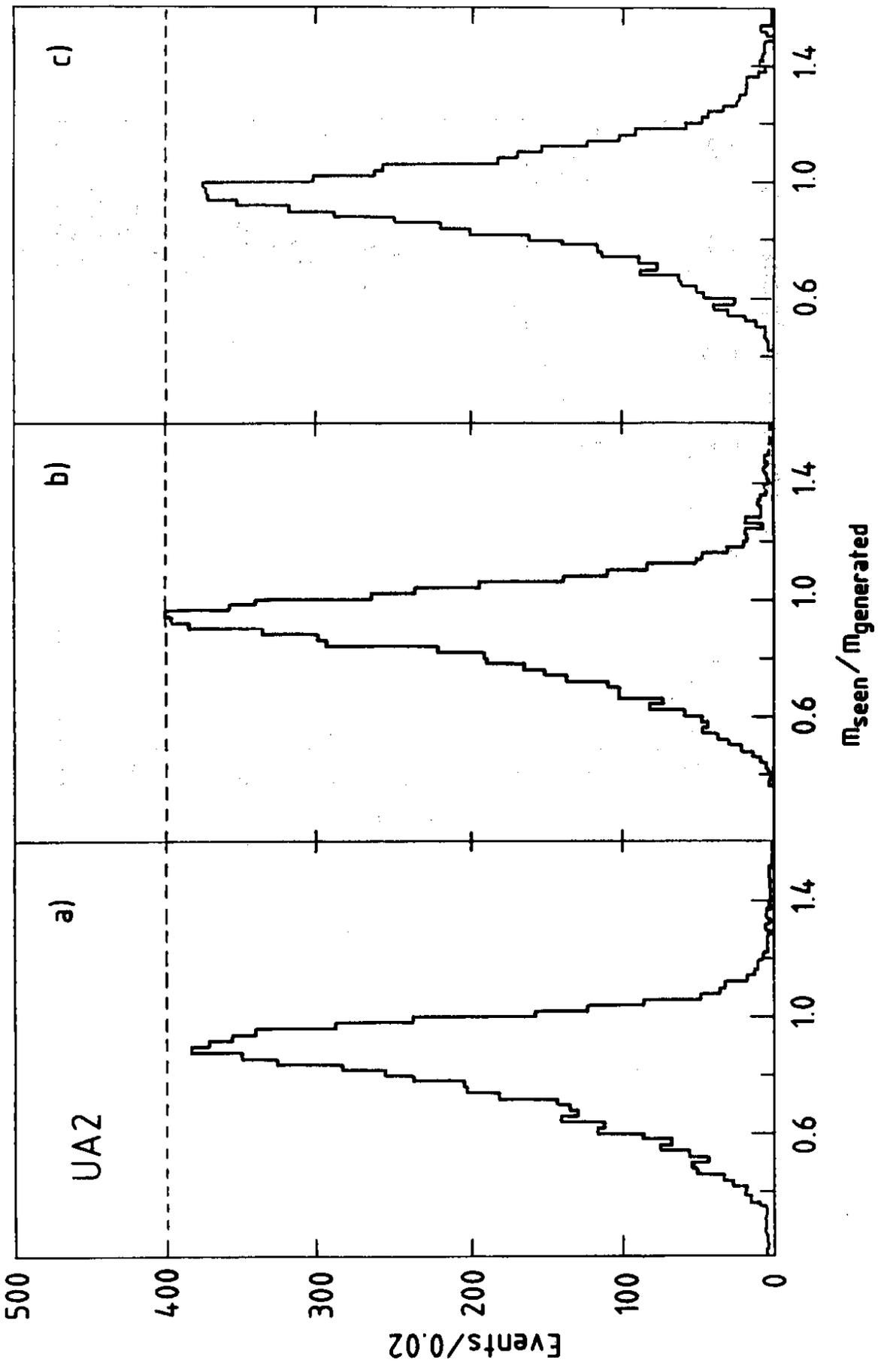
UA2
a)
b)
c)
Events/0.02
500
400
300
200
100
0
0.6
1.0
1.4
$m_{seen}/m_{generated}$

Fig. 1

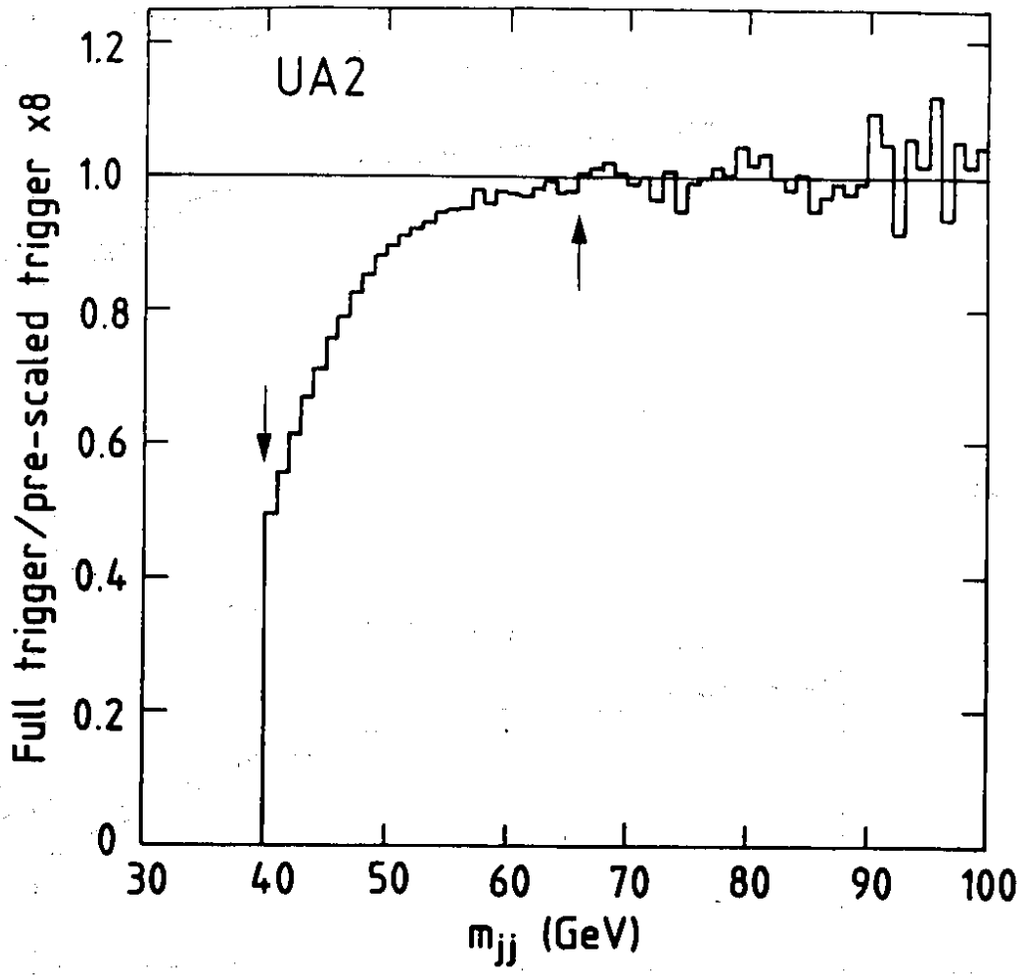
UA2
Full trigger/pre-scaled trigger x8
1.2
1.0
0.8
0.6
0.4
0.2
0
30
40
50
60
70
80
90
100
m_{jj} (GeV)

Fig. 2

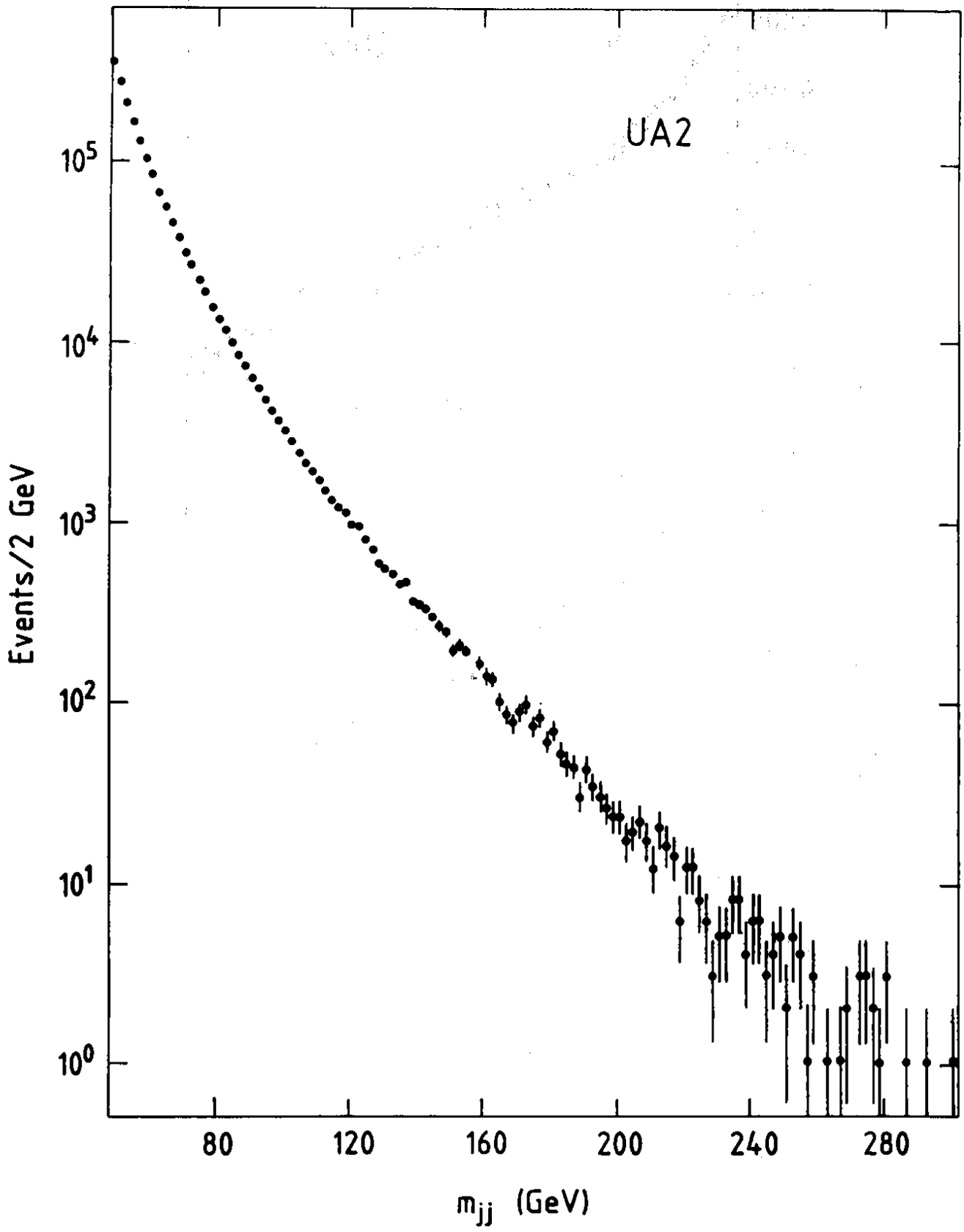
UA2
Events/2 GeV
10^5
10^4
10^3
10^2
10^1
10^0
80
120
160
200
240
280
m_{jj} (GeV)

Fig. 3

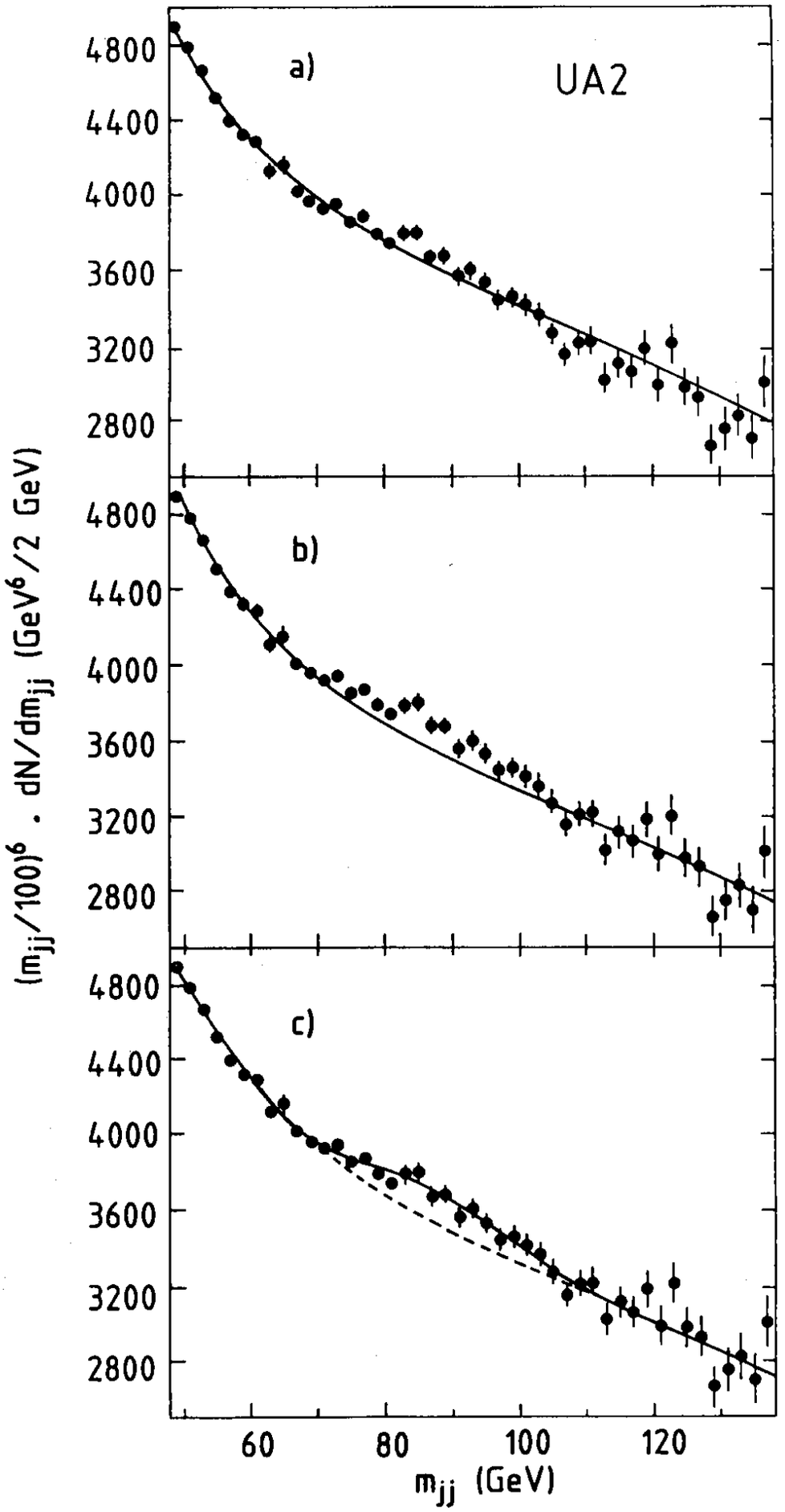
a)
UA2
b)
c)
4800
4400
4000
3600
3200
2800
60
80
100
120
m_{jj} (GeV)
$(m_{jj}/100)^6 \cdot dN/dm_{jj}$ (GeV^6/2 GeV)

Fig. 4

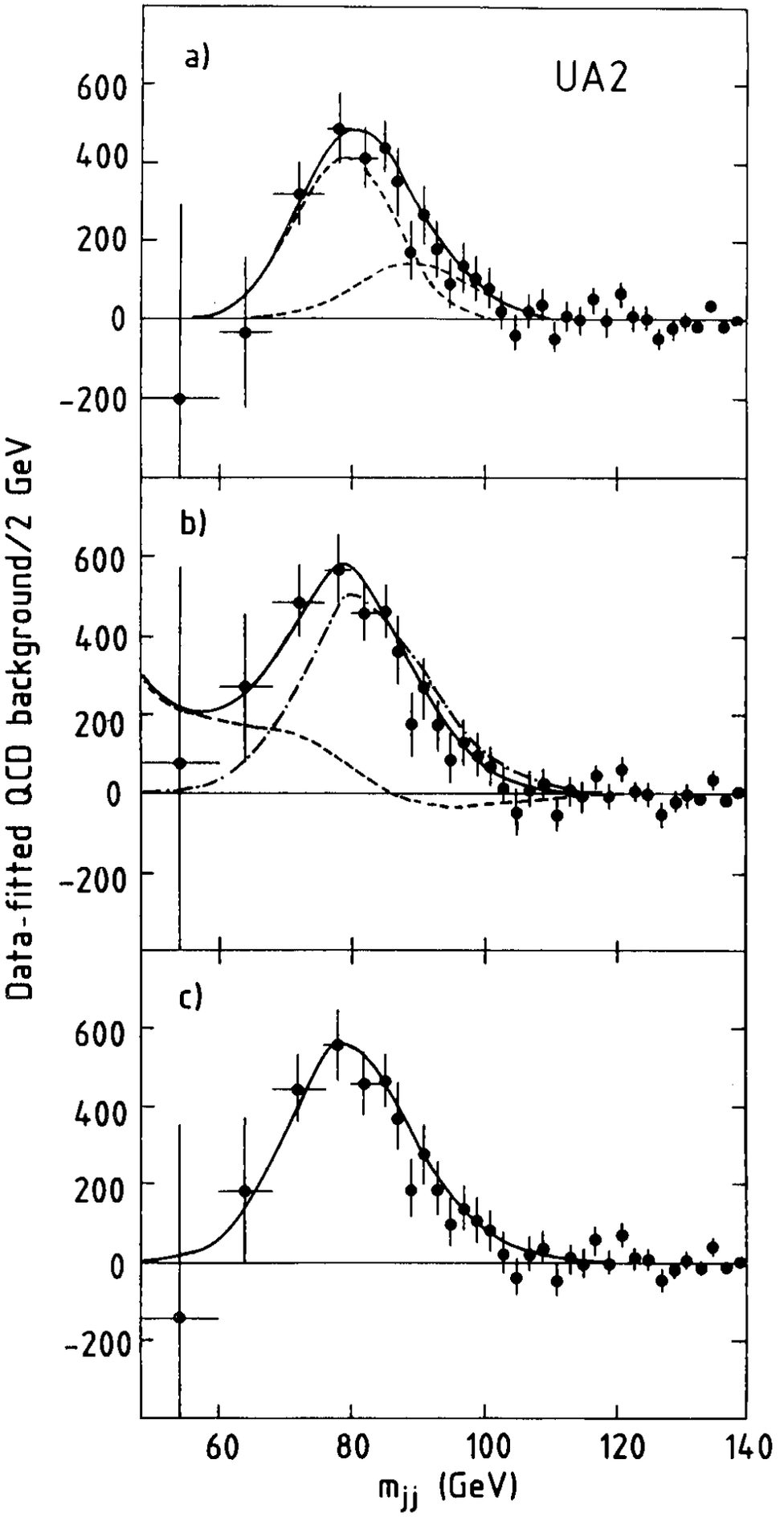
a)
UA2
b)
c)
600
400
200
0
-200
Data-fitted QCD background/2 GeV
60
80
100
120
140
m_{jj} (GeV)

Fig. 5

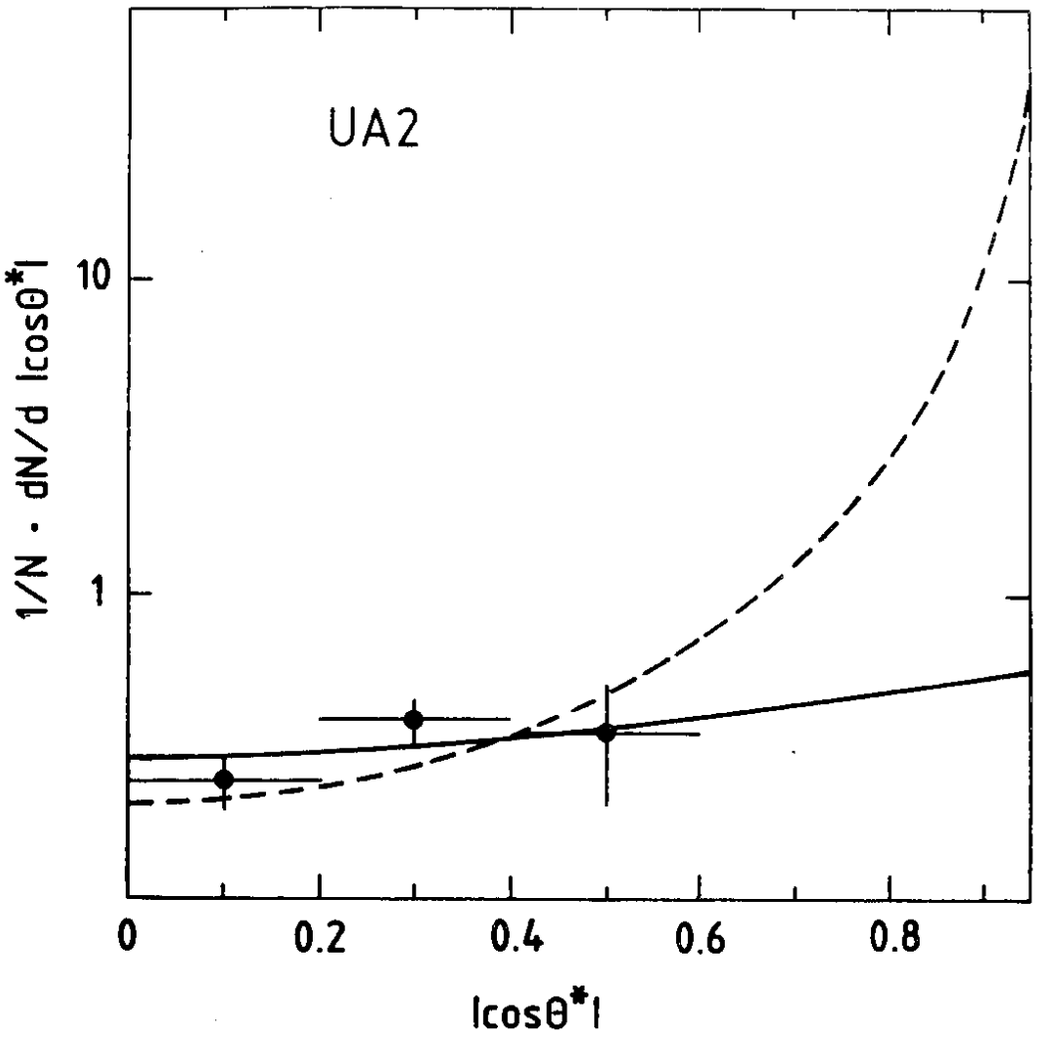

Fig. 6

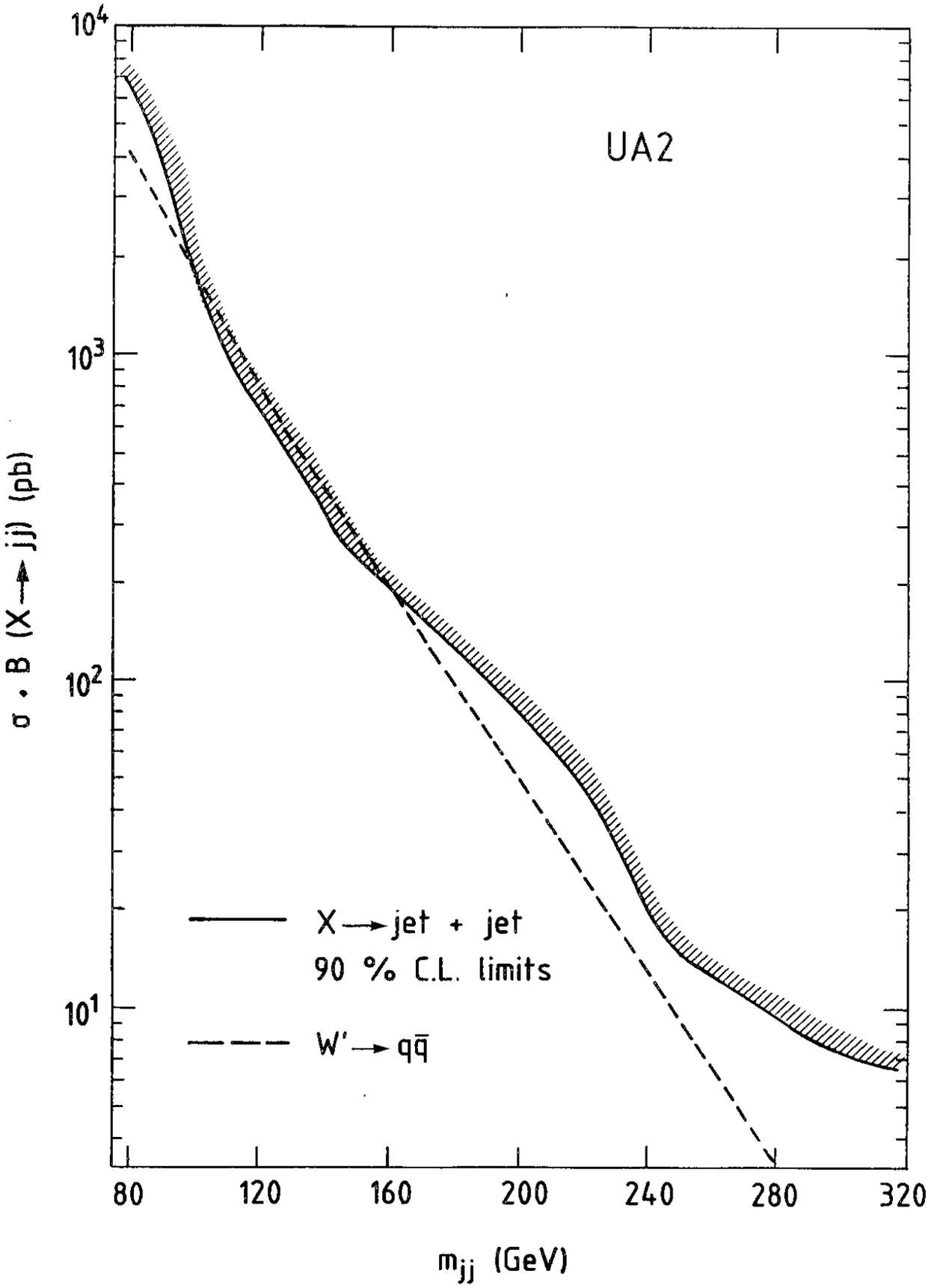

Fig. 7

Imprimé au CERN. Prix : 1.15 Fr.